Chemical Engineering Journal Advances 16 (2023) 100538

Contents lists available at ScienceDirect

Chemical Engineering Journal Advances

journal homepage: www.sciencedirect.com/journal/chemical-engineering-journal-advances

A multi-scale study of 3D printed Co-Al_2O_3 catalyst monoliths versus spheres

Clement Jacquot [a,b], Antonis Vamvakeros [c,d], Andraž Pavlišič [e], Stephen W.T. Price [c], Hongyang Dong [a,c], Dorota Matras [f,g], Lidia Protasova [b], Blaž Likozar [e], Simon D.M. Jacques [c], Andrew M. Beale [a,c,h], Vesna Middelkoop [b,*]

[a] Department of Chemistry, University College London, London WC1H 0AJ, United Kingdom
[b] Sustainable Materials Management, Flemish Institute for Technological Research (VITO), B-2400 Mol, Belgium
[c] Finden, Building R71, Harwell Campus, Oxfordshire, OX11 0QX, United Kingdom
[d] Dyson School of Design Engineering, Imperial College London, London SW7 2DB, United Kingdom
[e] Department of Catalysis and Chemical Reaction Engineering, National Institute of Chemistry, SI-1001 Ljubljana, Slovenia
[f] Diamond Light Source, Harwell Science and Innovation Campus, Didcot, Oxfordshire OX11 0DE, United Kingdom
[g] The Faraday Institution, Quad One, Harwell Science and Innovation Campus, Didcot,OX11 0RA, United Kingdom
[h] Research Complex at Harwell, Rutherford Appleton Laboratory, Harwell Science and Innovation Campus, Didcot, Oxon OX11 0FA, United Kingdom

ARTICLE INFO

Keywords:
3D printed catalyst monoliths
In situ synchrotron XRD-CT
Computational fluid dynamics (CFD)
Selective oxidation reaction
Multiphase reaction
Packed bed reactor

ABSTRACT

This study demonstrates the characteristics of two model packing configurations: 3D printed (3DP) catalyst monoliths on the one hand, and their conventional counterparts, packed beds of spheres, on the other. Cobalt deposited on alumina is selected as a convenient model system for this work, due to its wide spread use in many catalytic reactions. 3DP constructs were produced from alumina powder impregnated with cobalt nitrate while the alumina spheres were directly impregnated with the same cobalt nitrate precursor. The form of the catalyst, the impregnation process, as well as the thermal history, were found to have a significant effect on the resulting cobalt phases. Probing the catalyst bodies *in situ* by XRD-CT indicated that the level of dispersion of identified Co phases (Co_3O_4 reduced to CoO) across the support is maintained under reduction conditions. The packed bed of spheres exhibits a non-uniform distribution of cobalt phases, including a core-shell morphology with an average crystallite size of 10–14 nm across the sphere, while the 3DP monolith exhibits a uniform distribution of cobalt phases with an average crystallite size of 5–12 nm upon reduction from Co_3O_4 to CoO. Computational Fluid Dynamics (CFD) modelling was carried out to develop digital twins and assess the effect of the geometry of both configurations on the pressure drop and velocity profiles. Finally, the activity of both Cobalt-based catalyst geometries was assessed in terms of their conversion, selectivity and turn over frequencies under model multi-phase (selective oxidation) reaction conditions, which showed that the desired 3D printed monolithic geometries can offer distinct advantages to the reactor design.

1. Introduction

The substitution of platinum group metals (PGMs) by more earth abundant 3d transition or base metals present an attractive solution from a sustainability perspective although the latter tend to suffer from lower performance. One example is cobalt catalysts, which are one of the most commonly used and known to efficiently catalyse a great number of reactions due to cobalt's redox state and the possibility to optimise the nanoparticle size, rendering its performance similar to that of PGMs [1,2] However, improved performance can be obtained when optimising the shape, size and structure at both the nano- and macro-scales [3–5]. One of the main advantages of monolithic catalysts is that they offer low pressure drop and higher mass and heat transfer leading to the optimisation of the reactor design [6,7].

Owing to the flexibility of the 3D printing process, there has been considerable interest in monolithic reactors for a wide range of catalytic applications [8,9]. In this work the monoliths were 3D printed with straight-line geometry and uniform cell density. In the literature, whilst

* Corresponding author.
E-mail address: vesna.middelkoop@vito.be (V. Middelkoop).

https://doi.org/10.1016/j.ceja.2023.100538

Available online 26 July 2023

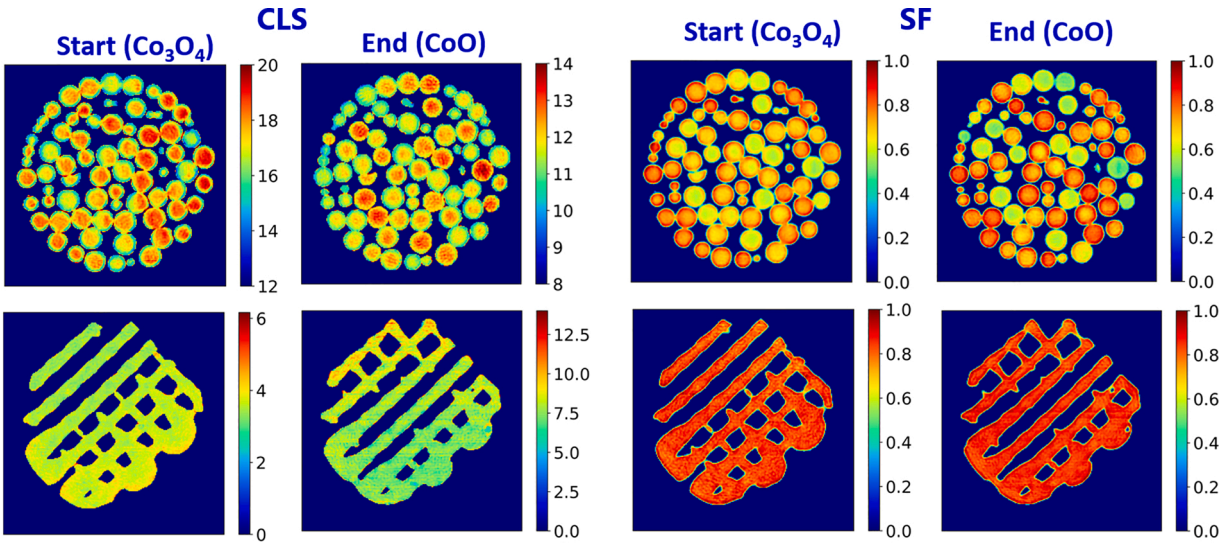

Fig. 1. Reconstructed 2D XRD-CT images of Cobalt phases across PB of spheres (top row) and 3DP monolith (bottom row) under 100 ml min^{-1} flow of 5% H_2 in He: (from left to right) average crystallite size (CLS), colour scale bar in nm, and scale factor (SF) 0–1; each set of images shows start of temperature ramp - Co_3O_4 (left) and end of temperature ramp at 400 °C - CoO (right).

there is a wealth of work on CFD modelling of fixed bed reactors [10,11], little work has been done on the direct comparison of 3D printed (3DP) monoliths and their packed bed (PB) counterparts [12,13]. The straight-channel monoliths were evaluated by Computational Fluid Dynamic (CFD) comparing their flow patterns and pressure drops for varied superficial velocities with that of PB of spheres.

The vast majority of *in situ* and *operando* studies in the literature utilise the traditional 0D single-point scans of catalysts in powdered form. We present here XRD-CT analysis of the entire 2D cross sections of both configurations of the Co-Al_2O_3 structured catalysts, 3DP catalyst monoliths and PB of spheres, recorded before and after reduction in H_2/He. This set of analysis tools enables the catalyst bodies to be 'chemically imaged' in spatial and temporal dimensions in order to provide a better understanding of the relationship between catalyst structure and function under operating conditions [14,15].

Finally, the activity of both catalyst forms has been tested in a model multiphase flow reaction (the selective oxidation of benzyl alcohol to benzaldehyde) that has been widely adopted in the chemical industry for its intermediate products [16,17]. However, the majority of selective oxidation reaction processes are operated in closed batches for large volumes, or, alternatively, in microchannel reactors for continuous flows at small scale. Building on their most recent work on the effects of 3DP geometries in different bimetallic FeCo@Al_2O_3 and FePd@Al_2O_3 compositions on catalytic performance [18], the authors demonstrate here that the conventional (batch and PB) PGM-based catalytic systems can be entirely replaced by cobalt while comparing 3DP monolithic catalyst beds with their PB analogues under identical operating conditions.

2. Materials and methods

The impregnation method and 3D printing (direct write) were previously described by the authors [19,20], (for further details see Supplementary Material).

XRD-CT measurements at the ESRF ID15A beamline [21] were performed in a quartz reactor tube (see Supplementary Figure S1) using a monochromatic beam of 89 keV focused to a spot size of 30 μm x 30 μm. XRD-CT scans were recorded using interlaced method [22]. Each complete interlaced scan comprised 39,600 diffraction patterns, each acquired over 10 msecs. 2D powder diffraction patterns were collected using a state-of-the-art Pilatus3 X CdTe 2 M hybrid photon counting area detector. The final XRD-CT images (i.e. reconstructed data volume) were processed using the filtered back projection algorithm and pyFAI and the nDTomo software suite [23–26].

The reactor set-up and conditions for the aerobic selective oxidation of benzyl alcohol into benzaldehyde were used as previously described by the authors [27]

CFD simulations were performed in open-source software openFOAM. First, spheres bed and monolith were fully digitally twined. For computational mesh (CM), a procedure was applied from previous work of the authors, which proved to be effective for grid-independent velocity field [27] . The final CM consisted of ~ 1 million elements for both geometries. All CFD simulations were conducted with k-w type Reynolds averaged model.

3. Results and discussion

3.1. *In situ* XRD-CT analysis

XRD-CT was used to image the spatial (and temporal) distribution of Cobalt phases across the catalysts. Fig. 1 shows the resulting, reconstructed 2D XRD-CT images of PB of Co-Al_2O_3 catalyst spheres and 3DP monoliths before and after reduction. The peak fitting results obtained according to the methods previously described by the authors [28,29] are explained in more detail in Supplementary Figures S2-S5. The parallax artefact was removed from the XRD-CT data using a 3D parallax Radon we previously developed for the DLSR approach [30]. Two reconstructions were obtained per XRD-CT dataset using the odd and even projections; the data were then denoised using the Noise2Inverse approach [31] with a 3D convolutional neural network (for more details regarding the reconstruction algorithm see the Supplementary Material section, Figures S6-S16).

Clear changes in diffraction patterns can be observed in both sets of temperature ramp data (for the PB of spheres see Fig. 1, top, and for 3DP monolith Fig. 1, bottom). Both Al_2O_3 supports are crystalline, however, the spheres are more crystalline than the printed sample which can be attributed to their different preparation methods (see Supplementary Figure S15 and Table S1). Fig. 1, top shows clearly crystalline Co_3O_4 in the spheres reducing to CoO. In contrast, Fig. 1, bottom, shows the Co_3O_4 to be less crystalline in the 3DP material reducing to less crystalline CoO.

Initially Co is present in spinel form, in 18–20 nm crystallites (Fig. 1,

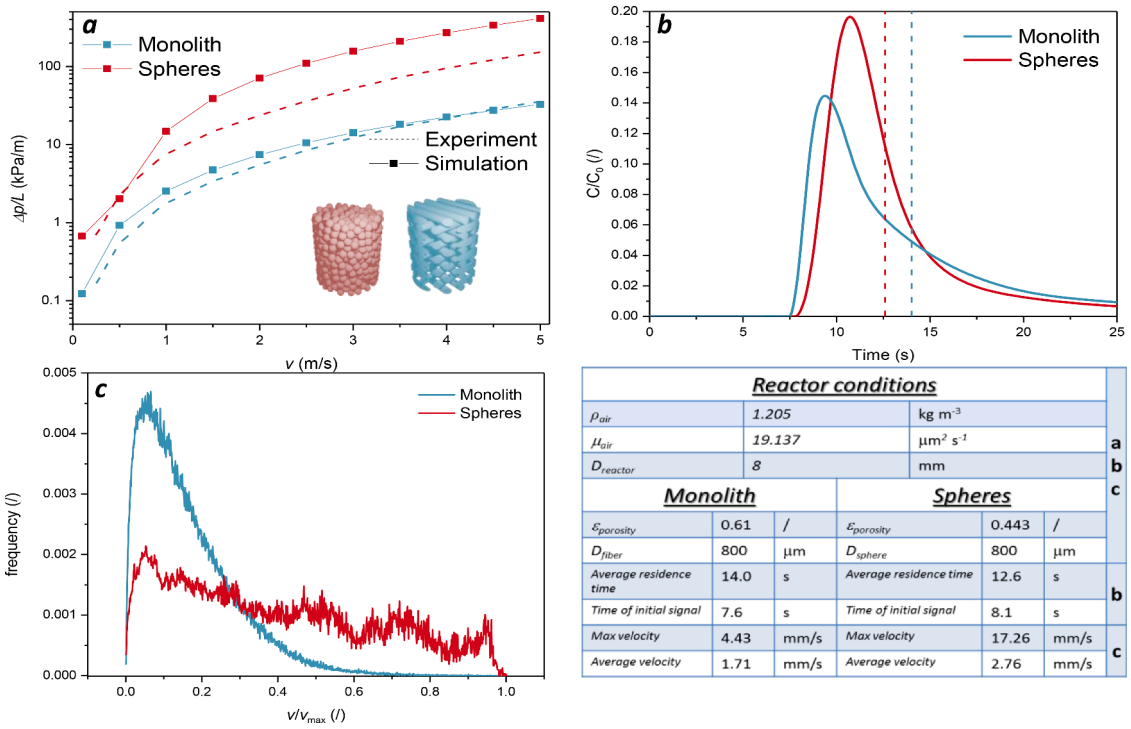

Reactor conditions			
ρ_{air}	1.205	kg m^{-3}	a
μ_{air}	19.137	μm^2 s^{-1}	b
$D_{reactor}$	8	mm	c

Monolith			Spheres			
$\varepsilon_{porosity}$	0.61	/	$\varepsilon_{porosity}$	0.443	/	
D_{fiber}	800	μm	D_{sphere}	800	μm	
Average residence time	14.0	s	Average residence time	12.6	s	b
Time of initial signal	7.6	s	Time of initial signal	8.1	s	
Max velocity	4.43	mm/s	Max velocity	17.26	mm/s	c
Average velocity	1.71	mm/s	Average velocity	2.76	mm/s	

Fig. 2. CFD results for PB of spheres and 3DP monolith: (a) Pressure drops for various superficial velocities. (b) Tracer test for superficial velocity of 1 mm/s. (c) Velocity distribution for superficial velocity of 1 mm/s.

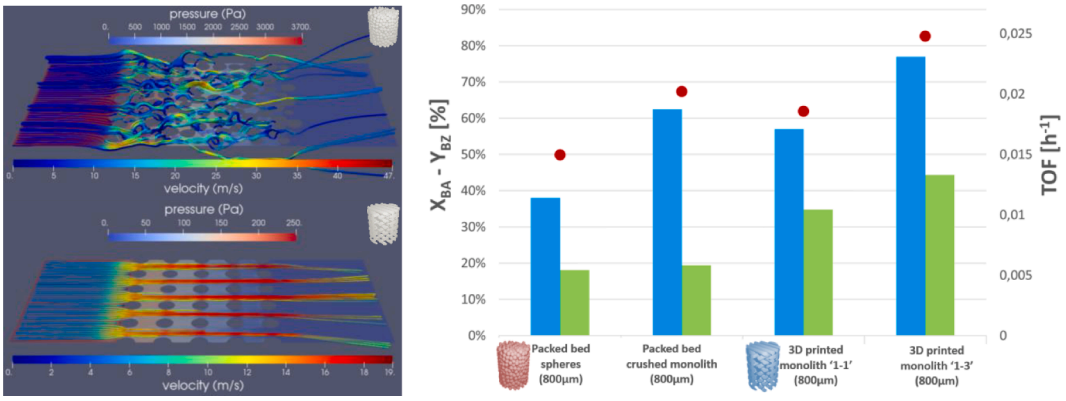

Fig. 3. Performance comparison for 3DP Co-Al_2O_3 monoliths (fibre thickness and interfibre distance of 800 μm) with their PB analogues (spheres and 3DP crushed catalysts fractions of around 800 μm) - Left panel: stream lines and pressure drops for spheres (top) and monolith (bottom) at superficial velocity of 5 m/s. Right panel: benzyl alcohol oxidation in flow reactor; Legend: X_{BA}( ) corresponds to conversion of benzyl alcohol; S_{BZ}( ) corresponds to selectivity into benzaldehyde; TOF ( ) is turn-over frequency, expressed in h^{-1}.

top left), with some variation in lattice parameters across the PB of spheres (Figure S16). The Co_3O_4 is almost fully converted to CoO by the end of the ramp. The reduction in size (from ca. 12–20 nm to 10–14 nm) is expected due to the loss of oxygen from the lattice. Cobalt crystallite sizes appear independent of support crystallite size. There may be some movement of Co in spheres as clustering of larger CoO crystallite sizes appears to have occurred. This points to tentative correlation with larger support crystallites.

Both the average crystallite size (CLS) images in Fig. 1, top left and scale factor (SF) images in Fig. 1, top right, show a non-uniform distribution of Cobalt phases across the PB of spheres, including a core-shell distribution for individual spheres which is supported by SEM/EDX images (Figure S18). In contrast, a homogeneous distribution of Cobalt phases can be observed across the 3DP monolith in both the CLS (Fig. 1, bottom left) and SF (Fig. 1, bottom right) images, which is confirmed by the SEM/EDX results (Figure S19). This underlines the fact that 3D printing offers greater control and uniform distribution of the active catalyst material. Upon reduction from Co_3O_4 to CoO, the average CLS is expected to decrease if Co dispersion in the support is maintained. However, in this case, the Co average CLS per pixel in the 3DP monolith is shown to increase from ca. 2–6 nm to 5–12 nm (Fig. 1, bottom left). This may be indicative of some sintering, or, as previously stated, it may be due to poor crystallinity.

3.2. CFD analysis

The pressure drop of the spheres and monolith configurations is presented in Fig. 2a. As expected, the pressure drop for spheres is substantially higher than that for monoliths for the same characteristic dimension (i.e. spheres and fibre diameter of 800 mm). This is mainly

due to higher porosity of monolith, which leads to lower average velocity and consequently lower viscous losses (see Fig. 2c). In addition, the flow pattern in monolith follows creeping flow, while in case of spheres the flow is more swirly, which leads to higher inertia loses and consequently higher pressure drop (see Fig. 3 left panel). While this is a well-known fact, it is not straightforward to deduce the impact of geometry on the heat and mass transfer solely from the experiments. Therefore, a detailed CFD tracer test analysis of residence time was performed (see Fig. 2b). Even though the average velocity in case of spheres is higher than monolith, the residence time of the initial signal is shifted to later time than monolith, meaning that spheres have higher tortuosity than monolith and consequently more inertia losses. In contrast, the average residence time of monoliths is higher than that of spheres which leads to higher conversion rates.

3.3. Catalytic testing in model selective oxidation reaction

The present study exhibits a geometry dependency for Co-Al_2O_3 in the selected model reaction. When formed into monolithic catalysts by 3D printing, Co-Al_2O_3 showed higher conversion, selectivity and turn over frequency (TOF) during the benzyl alcohol oxidation to benzaldehyde over the same range of reaction conditions. Equivalent experiments were performed in the flow reactor using not only catalyst spheres but also 3DP catalyst in a crushed (and pelletised) form (see comparison results in Fig. 3, right panel). 3DP monoliths with the straight channels (designated "1–1″) exhibited conversion rates and TOF comparable to their crushed counterparts while the catalyst spheres have the lowest conversion and TOF. The 3D-printed monoliths with crossed channels (designated "1–3″) had a higher conversion rate (78%) and TOF (0.025 h^{-1}) than those of monoliths with straight channels. Further optimisation of 3D printed monoliths' (crossed channel) geometry and their performance in terms of conversion, selectivity and TOF, was successfully demonstrated (see Supplementary Figures S20 and S21).

4. Conclusions

A model alumina-supported cobalt catalyst was 3DP into a monolith with straight channels and examined together with its counterpart, conventional PB of model spheres. The effect of the packing geometry was studied by directly comparing CFD and experimental data for the pressure drop and velocity profiles of the respective configurations. The pressure drop in the PB of spheres was significantly higher in comparison to that in the monolithic reactor considering the characteristic dimensions are the same (i.e. monolith filament and spacing of 800 μm and sphere diameter of 800 μm). This is attributed to the higher porosity of the monolith, which leads to lower average velocity and consequently lower viscous losses.

Secondly, the application of complementary in situ and *ex situ* techniques (such as XRD-CT and SEM-EDX) is invaluable in assessing the fidelity of the printing process and mapping the catalyst chemical form, microstructure and behaviour. The reconstructed images of the in situ XRD-CT measurements under H_2 flow show (from the nano and micro to macro scale) the differences in the distribution and level of crystallinity and particle size of cobalt species between the spheres and the printed sample. The 3DP monolith exhibits a uniform distribution of cobalt phases throughout the cross section while non-uniform distribution is observed across the packed-bed of spheres including their core-shell morphology.

Lastly, the model packings were compared under model reaction conditions of the selective oxidation of benzyl alcohol to benzaldehyde. The monoliths with straight channels showed conversion rates and TOF that were equivalent to those of their crushed PB counterparts, whereas the catalyst spheres had the lowest TOF and conversion. The optimised geometry and obtained performance of 3DP Co-Al_2O_3 monoliths with crossed channels (detailed in the Supplementary Material section) reached 90% conversion of benzyl alcohol (0.029 h^{-1} TOF), demonstrating their potential to replace both the traditional PB configurations and PGM-based catalytic systems. This illustrates that 3D printing of catalyst monoliths allows great control over the active material distribution, flow pathways, reaction times and higher surface area to volume ratio for the reactants, facilitating easy set-up, scale-up and ultimately reaction optimisation.

CRediT authorship contribution statement

Investigation, Methodology, Validation, Vizualisation: C.J., L.P and V.M. carried out the synthesis/materials preparation, catalytic testing and conventional characterisation. A.P. and B.L. performed CFD modelling and interpretation. V.M., D.M. and S.D.M.J. designed and performed the XRD-CT experiments with contributions from A.V. and A. M.B. A.V. and H.D. developed the iterative GPU-based parallax reconstruction approach used in this work. Software, Visualization: A.V. developed and applied the code for the self-supervised denoising approach used in this work with contributions from H.D. XRD-CT data interpretation was performed by A.V., H.D., V.M. and S.W.T.P. with contributions from S.D.M.J. and A.M.B. A.V. performed the full profile analysis of the XRD-CT data with contributions from S.W.T.P. and V.M. Writing - review&editing: all authors made contributions to writing and editing the manuscript.

Declaration of Competing Interest

The authors declare that they have no known competing financial interests or personal relationships that could have appeared to influence the work reported in this paper.

Data availability

We have published the sinogram data only on https://zenodo.org/record/8116842 (DOI: 10.5281/zenodo.8116842).

Acknowledgements

All the authors also gratefully acknowledge the financial support provided by their respective institutions. The authors would like to thank Myrjam Mertens, Kosar Hassannezhad (lab XRD), Raymond Kemps, Nancy Dewit (SEM/EDX), Anne-Marie De Wilde (N2 adsorption), Filip Beutels (ICP) and Diane Bertels (HPLC). The authors wish to acknowledge Sasol Performance Chemicals, Inorganics & Catalysts Division, Germany for kindly supplying commercial alumina spheres. We would like to particularly thank ESRF for beamtime (CH4782) and Marco di Michiel (ID15A, ESRF) for preparing beamline instrumentation and setup and for his help with the experimental XRD-CT data acquisition. Antonis Vamvakeros acknowledges financial support from the Royal Society as a Royal Society Industry Fellow (IF\R2\222059).

Supplementary materials

Supplementary material associated with this article can be found, in the online version, at doi:10.1016/j.ceja.2023.100538.

References

[1] Pierre Senecal, Simon D.M. Jacques, Marco Di Michiel, Simon A.J. Kimber, Antonis Vamvakeros, Yaroslav Odarchenko, Ines Lezcano-Gonzalez, James Paterson, Ewen Ferguson, Andrew M. Beale, Real-time scattering-contrast imaging of a supported cobalt-based catalyst body during activation and Fischer-Tropsch synthesis revealing spatial dependence of particle size and phase on catalytic properties, ACS Catal. 7 (4) (2017) 2284–2293.

[2] M. Rahmati, B. Huang, M.K. Mortensen, K. Keyvanloo, T.H. Fletcher, B. F. Woodfield, W.C. Hecker, M.D. Argyle, Effect of different alumina supports on performance of cobalt Fischer-Tropsch catalysts, J. Catal. 359 (2018) 92–100, https://doi.org/10.1016/j.jcat.2017.12.022.

[3] W.E. Bambrick, (1986). Improved shape for extruded catalyst support particles and catalysts. EP86113184A1. Munich: European patent office.
[4] G. Do, M. Geißelbrecht, W. Schwieger, H. Freund, Additive manufacturing of interpenetrating periodic open cellular structures (interPOCS) with in operando adjustable flow characteristics, Chem. Eng. Process. - Process Intensification 148 (2020), 107786, https://doi.org/10.1016/j.cep.2019.107786.
[5] Z. Dong, Z. Wen, F. Zhao, S. Kuhn, T. Noel, T. scale-up of micro- and milli-reactors: an overview of strategies, design principles and applications, Chem. Eng. Sci. 10 (2021), 100097, https://doi.org/10.1016/j.cesx.2021.100097.
[6] S. Afandizadeh, E.A. Foumeny, Design of packed bed reactors: guides to catalyst shape, size and loading selection, Appl. Therm. Eng. 21 (2001) 669–682, https://doi.org/10.1016/S1359-4311(00)00072-7.
[7] Leon R.S. Rosseau, Vesna Middelkoop, Hans A.M. Willemsen, Roghair Martin van Sint Annaland, Review on additive manufacturing of catalysts and sorbents and the potential for process intensification, Front. Chem. Eng. (2022) 4, https://doi.org/10.3389/fceng.2022.834547.
[8] X. Zhou, C. Liu, C. Three-dimensional printing for catalytic applications: current status and perspectives, Adv. Funct. Mater. 27 (2017), 1701134.
[9] Shane Lawson, Xin Li, Harshul Thakkar, Ali A. Rownaghi and Fateme Rezaei, Recent advances in 3D printing of structured materials for adsorption and catalysis applications chemical reviews 2021, 121 (10), 6246–6291.
[10] S.H. Cheng, H. Chang, Y.H. Chen, H.J. Chen, Y.K. Chao, Y.H. Liao, Computational fluid dynamics-based multiobjective optimization for catalyst design, Ind. Eng. Chem. Res. 49 (2010) 11079–11086, https://doi.org/10.1021/ie1001839.
[11] K.G. Allen, T.W. von Backström, D.G. Kröger, Packed bed pressure drop dependence on particle shape, size distribution, packing arrangement and roughness, Powder Technol. 246 (2013) 590–600, https://doi.org/10.1016/j.powtec.2013.06.022.
[12] V. Middelkoop, A. Vamvakeros, D. De Wit, S. Jacques, S. Danaci, C. Jacquot, Y. De Vos, S.Price D.Matras, A. Beale, 3D printed Ni/Al2O3 based catalysts for CO2 methanation: a comparative and operando XRD-CT study, J. CO2 Utilization 33 (2019) 478–487.
[13] V. Middelkoop, K. Coenen, J. Schalck, M. Van Sint Annaland, F. Gallucci, 3D printed versus spherical adsorbents for gas sweetening, Chem. Eng. J. 357 (2019) 309–319.
[14] A.M. Beale, S.D.M. Jacques, E.K. Gibson, M. Di Michiel, Coordination chemistry reviews, progress towards five dimensional diffraction imaging of functional materials under process conditionsCoordin, Chem. Rev. 277 (2014) 208–223.
[15] Dorota Matras, Jay Pritchard, Antonios Vamvakeros, Simon D.M. Jacques, Andrew M. Beale, Tomography in catalyst design, heterogeneous catalysts: advanced design, characterization and applications, II, Book Editor(s):Wey Yang Teoh, Atsushi Urakawa, Yun Hau Ng, Patrick Sit, 2021 10.1002/9783527813599.ch15.
[16] F. Galvanin, M. Sankar, S. Cattaneo, D. Bethell, V. Dua, G.J. Hutchings, A. Gavriilidis, On the development of kinetic models for solvent-free benzyl alcohol oxidation over a gold-palladium catalyst, Chem. Eng. J. 342 (2018) 196–210, https://doi.org/10.1016/j.cej.2017.11.165.
[17] Qi Han, Xian-Tai Zhou, Xiao-Qi He, Hong-Bing Ji, Mechanism and kinetics of the aerobic oxidation of benzyl alcohol to benzaldehyde catalyzed by cobalt porphyrin in a membrane microchannel reactor, Chem. Eng. Sci. 245 (2021), 116847.
[18] Clément Jacquot, Vesna Middelkoop, Angela Köckritz, Andrej Pohar, Regina Bienert, Suela Kellici, Ioan-Alexandru Bărăgău, Baldassarre Venezia, Asterios Gavriilidis, Blaz Likozar, Andrew M. Beale, 3D printed catalytic reactors for aerobic selective oxidation of benzyl alcohol into benzaldehyde in continuous multiphase flow, Sustain. Mater. Technol. 30 (2021) e00329.
[19] V. Middelkoop, T. Slater, M. Florea, F. Neațu, S. Danaci, V. Onyenkeadi, K. Boonen, B. Saha, S.Kellici IA.Baragau, Next frontiers in cleaner synthesis: 3D printed graphene-supported CeZrLa mixed-oxide nanocatalyst for CO2 utilisation and direct propylene carbonate production, J. Clean. Prod. 214 (2019) 606–614.
[20] T. Karsten, V. Middelkoop, D. Matras, A. Vamvakeros, S. Poulston, V. Grosjean, B. Rollins, H.R.Godini F.Gallucci, S.D.M. Jacques, A.M. Beale, J.U. Repke, Multi-scale studies of 3D printed Mn-Na-W/SiO2 catalyst for oxidative coupling of methane, Catalysts 11 (3) (2021) 290.
[21] G.B.M. Vaughan, R. Baker, R. Barret, J. Bonnefoy, T. Buslaps, S. Checchia, D. Duran, F. Fihman, P. Got, J. Kieffer, S.A.J. Kimber, K. Martel, C. Morawe, D. Mottin, E. Papillon, S. Petitdemange, A. Vamvakeros, J.P. Vieux, M. Di Michiel, ID15A at the ESRF - a beamline for high speed operando X-ray diffraction, diffraction tomography and total scattering, J. Synchrotron Rad. 27 (2020) 515–528, https://doi.org/10.1107/S1600577519016813.
[22] S.D.M.Jacques Vamvakeros, M. Di Michiel, P. Senecal, V. Middelkoop, R.J. Cernik, A.M. Beale, Interlaced X-ray diffraction computed tomography, J. Appl. Cryst. 49 (2016) 485–496.
[23] G. Ashiotis, A. Deschildre, Z. Nawaz, J.P. Wright, D. Karkoulis, F.E. Picca, J. Kieffe, The fast azimuthal integration Python library: pyFAI, J. Appl. Cryst. 48 (2015) 510–519, https://doi.org/10.1107/S1600576715004306.
[24] J. Kieffer, S. Petitdemange, T. Vincent, Real-time diffraction computed tomography data reduction, J. Synchrotron Rad. 25 (2018) 612–617, https://doi.org/10.1107/S1600577518000607.
[25] Vamvakeros, S.D.M. Jacques, M. Di Michiel, V. Middelkoop, C.K. Egan, R.J. Cernik, A.M. Beale, Removing multiple outliers and single-crystal artefacts from X-ray diffraction computed tomography data, J. Appl. Cryst. 48 (2015) 1943–1955, https://doi.org/10.1107/S1600576715020701.
[26] Vamvakeros, A. nDTomo software suite. 2018. Available online: https://github.com/antonyvam/nDTomo.
[27] Andraž Pavlišič, Rok Ceglar, Andrej Pohar, Blaž Likozar, Comparison of computational fluid dynamics (CFD) and pressure drop correlations in laminar flow regime for packed bed reactors and columns, Powder Technol., 328, 130–139, 10.1016/j.powtec.2018.01.029.
[28] Vesna Middelkoop, Christopher J. Tighe, Suela Kellici, Robert I. Gruar, James M. Perkins, Simon D.M. Jacques, Paul Barnes, Jawwad A. Darr, Imaging the continuous hydrothermal flow synthesis of nanoparticulate CeO2 at different supercritical water temperatures using in situ angle-dispersive diffraction, J Supercrit Fluids 87 (2014) 118–128.
[29] Stephen W.T. Price, David J. Martin, Aaron D. Parsons, Wojciech A. Sławiński, Antonios Vamvakeros, Stephen J. Keylock, Andrew M. Beale, J. Frederick, W. Mosselmans, Chemical imaging of Fischer-Tropsch catalysts under operating conditions, Sci. Adv. 3 (2017) 3, https://doi.org/10.1126/sciadv.160283.
[30] A.A.Coelho Vamvakeros, D. Matras, H. Dong, Y. Odarchenko, S.W.T. Price, K. T. Butler, O. Gutowski, A.C. Dippel, M. Zimmermann, I. Martens, J. Drnec, A. M. Beale, S.D.M. Jacques, DLSR: a solution to the parallax artefact in X-ray diffraction computed tomography data, J. Appl. Cryst. 53 (2020) 1531–1541, https://doi.org/10.1107/S1600576720013576.
[31] Hendriksen, D.M. Pelt, K.J. Batenburg, Noise2Inverse: self-supervised deep convolutional denoising for tomography, IEEE Trans. Comput. Imaging 6 (2020) 1320–1335, https://doi.org/10.1109/TCI.2020.3019647.